Role of proline, cysteine and a disulphide bridge in the structure and activity of the anti-microbial peptide gaegurin 5

Sang-Ho PARK, Hyung-Eun KIM, Chi-Man KIM, Hee-Jeong YUN, Eung-Chil CHOI and Bong-Jin LEE[1]

Research Institute of Pharmaceutical Sciences, College of Pharmacy, Seoul National University, Seoul 151-742, South Korea

Gaegurin 5 (GGN5) is a cationic 24-residue anti-microbial peptide isolated from the skin of a Korean frog, *Rana rugosa*. It contains a central proline residue and an intra-residue disulphide bridge in its C-terminus, which are common to the anti-microbial peptides found in Ranidae. We determined the solution structure of GGN5 bound to SDS micelles for the first time and investigated the role of proline, cysteine and a disulphide bridge on the structure and activity of GGN5. GGN5 adopts an amphipathic α-helical structure spanning residues 3–20 kinked around Pro-14, which allows the hydrophobic residues to reside in the concave helical region, and a disulphide-bridged loop-like conformation in its C-terminus. By replacement of proline with alanine (^{PA}GGN5), a straight and rigid helix was formed in the central region and was more stable than the kinked helix. Reduction of a disulphide bridge in the C-terminus (GGN5^{SH}) maintained the loosely ordered loop-like conformation, while the replacement of two cysteines with serines (^{CS}GGN5) caused the C-terminal conformation to be completely disordered. The magnitude of anti-microbial activity of the peptides was closely related to their helical stability in the order ^{PA}GGN5 > GGN5 > GGN5^{SH} > ^{CS}GGN5, suggesting that the helical stability of the peptides is important for anti-microbial activity. On the other hand, the significant increase of haemolytic activity of ^{PA}GGN5 implies that a helical kink of GGN5 could be involved in the selectivity of target cells. The location of GGN5 and ^{PA}GGN5, analysed using paramagnetic probes, was mainly at the surface of SDS micelles, although the location of the N-terminal region was slightly different between them.

Key words: helical kink, loop-like conformation, micelle-bound peptide fold, solution structure.

INTRODUCTION

Anti-microbial peptides are an integral part of the non-specific immune defence system [1]. In many cases, they are released from secretory glands into internal body fluids or on to mucosal epithelia at the site of inflammation. Many different families of anti-microbial peptides have been isolated in all living organisms, including insects, plants, animals and micro-organisms [2]. A number of peptides from the skin of various amphibians also have been found to have a broad spectrum of anti-microbial activities [3–9]. To combat the increasing emergence of drug-resistant bacteria, anti-microbial peptides have become a potential source of new antibiotics.

Gaegurins (GGNs), isolated from the skin of a Korean frog, *Rana rugosa*, manifest a broad spectrum of anti-microbial activity against various micro-organisms, but show very little or no haemolytic activity [10]. These peptides are classified into two families based on their sequence. Family I includes GGN1–4, which are composed of 33–37 amino acids. Family II includes GGNs 5 and 6, which are composed of 24 amino acids and contain a proline at the 14th position near the centre of the sequence. All GGNs contain two invariant cysteine residues, one at their C-terminus and the other at the seventh position from the C-terminus. The heptapeptide motif containing these two cysteine residues was linked by an intra-residue disulphide bridge, which was conserved in the anti-microbial peptides derived from others of the genus *Rana*, such as brevinins, esculentins and ranalexin [4–6].

Recently we have documented that the C-terminal disulphide bridge of GGN4 did not have an important role in the structure and activity of GGN4 [11]. It was also reported that the disulphide bridge of ranalexin did not affect significantly the structure and activity of ranalexin [12]. In these studies, the structure and activity of the oxidized and reduced form of the peptides were compared, but the precise role of the cysteine residues themselves in the function of the peptides was not investigated.

Although proline residues generally create a rigid bend in the peptide backbone, they are commonly found within the amphipathic helices of many anti-microbial peptides, such as melittin, alamethicin and buforin II, as well as the peptides isolated from the Ranidae. The importance of proline residues in the structure and activity of several anti-microbial peptides has been investigated. Replacement of a proline with an alanine decreased the anti-microbial activity of a GGN6 derivative [13,14] and buforin II [15,16], or increased the haemolytic activity without decreasing anti-microbial activity of melittin [17,18], a 16-residue model peptide [19] and alamethicin [20].

To investigate the contribution of proline, cysteine and a disulphide bridge to the structure and activity of GGN5, we prepared GGN5 and its three analogues, a Pro-14→Ala-substituted form (^{PA}GGN5), a Cys-18/Cys-24→Ser-substituted form (^{CS}GGN5) and a reduced form (GGN5^{SH}). Here we compared

Abbreviations used: DPC, dodecylphosphocholine; DTT-d_{10}, perdeuterated dithiothreitol; DQF, double-quantum filtered; GGN, gaegurin; GGN5^{SH}, reduced form of GGN5; ^{CS}GGN5, Cys-18/Cys-24→Ser-substituted form of GGN5; ^{PA}GGN5, Pro-14→Ala-substituted form of GGN5; RMSD, root-mean-square deviation; methanol-d_4, perdeuterated methanol; SDS-d_{25}, perdeuterated SDS; 2D, two-dimensional; TFE, trifluoroethanol; NOESY, nuclear Overhauser enhancement spectroscopy; NOE, nuclear Overhauser effect.

[1] To whom correspondence should be addressed (e-mail lbj@nmr.snu.ac.kr).

the solution structure of GGN5 and its analogues in SDS micelles using CD and NMR spectroscopy, and studied the effects of substitution of proline with alanine and cysteine with serine on the anti-microbial and haemolytic activity of GGN5. In addition, we determined the location of GGN5 and ^{PA}GGN5 in SDS micelles using Mn^{2+} ions and spin-labelled 5- and 12-doxyl stearic acids as paramagnetic probes. Structural and functional implications of a helical kink and C-terminal disulphide bridge in the anti-microbial peptide GGN5 are discussed.

EXPERIMENTAL

Peptides and materials

Three peptides, GGN5, ^{PA}GGN5 and ^{CS}GGN5, were purchased from AnyGen Co., Kwang Ju, South Korea. The purity of the peptides was assessed by HPLC equipped with a reversed-phase C_{18} analytical column. The samples were eluted with a linear gradient of acetonitrile from 40 to 60 %, in the presence of 0.1 % trifluoroacetic acid at a flow rate of 1 ml/min over 45 min. Absorbance was monitored at 214 nm. The MS data (electrospray ionization) of GGN5, ^{PA}GGN5 and ^{CS}GGN5 were in agreement with the expected sequences, i.e. 2552, 2526 and 2520 Da, respectively. The sequences of the peptides are shown in Table 1. Perdeuterated SDS (SDS-d_{25}) and dithiothreitol (DTT-d_{10}) were obtained from Isotec. 5- and 12-doxyl stearic acids were from Sigma. $MnCl_2$, perdeuterated methanol (methanol-d_4) and sodium 4,4-dimethyl-4-silapentane-1-sulphonate were from Aldrich. All other chemicals were of analytical grade obtained from various manufacturers.

Anti-microbial and haemolytic assays

Anti-microbial activities of the peptides were determined by measuring the minimal inhibitory concentration for diverse micro-organisms, as described previously [10]. To estimate the effect of dithiothreitol on anti-microbial activity, the control experiment without peptide was performed. Addition of even 10 mM dithiothreitol to bacteria did not affect the bacterial growth. The minimal inhibitory concentration against various bacteria was determined by incubating 10^6 colony-forming units/ml of cells in Luria–Bertani media including variable amounts of peptides. Cell growth was quantified by measuring the D_{600} of the culture suspension. Haemolysis induced by each peptide was determined by incubating a 10 % (v/v) suspension of human red blood cells in PBS with the appropriate amount of each peptide at 37 °C for 30 min. After centrifugation at 10000 ***g*** for 10 min, the D_{550} of the supernatant was measured. The relative attenuance compared with that of the suspension treated with 0.2 % Triton X-100 was defined as the percentage of haemolysis.

Table 1 Sequence alignment of GGN5 and its analogue peptides with three other anti-microbial peptides from the Ranidae

The intra-residue disulphide bridge of the heptapeptide motif in the C-terminus is depicted with underlining and the conserved amino acids, except in GGN4 and the analogues of GGN5, are denoted in bold. The substituted amino acids of the analogues of GGN5 are shown in italics.

Peptide	Amino acid sequence
GGN4	[1]GILDTLKQFAKGVGKDLVKGAAQGVLSTVSCKLAKTC
GGN5	[1]**FL**GA**L**FKVASKVL**P**SVK**C**AITK**KC**
GGN6	[1]**FL**PL**L**AGLAANFL**P**TII**C**FISY**KC**
Brevinin 1E	[1]**FL**PL**L**AGLAANFL**P**KIF**C**KITR**KC**
Ranalexin	[1]**FL**GG**L**----IKIV**P**AMI**C**AVTK**KC**
^{PA}GGN5	[1]FLGALFKVASKVL*S*VK*C*AITKKC
^{CS}GGN5	[1]FLGALFKVASKVLPSVK*S*AITKK*S*

CD spectroscopy

For CD experiments, GGN5 and its analogues were prepared by dissolving the lyophilized peptides to a concentration of 50 μM in various solvents: aqueous buffer, trifluoroethanol (TFE)/water mixture, SDS micelles and dodecylphosphocholine (DPC) micelles. All samples were tested at both pH 6.0 and pH 4.0. CD spectra were obtained by using a JASCO J-715 spectropolarimeter equipped with a Peltier temperature controller, using a 2 mm-pathlength cell, with a 1 nm bandwidth, 0.5 nm resolution, 2 s response time and a scan speed of 50 nm/min. The spectra were measured from 250 to 190 nm at 25 °C. Three scans were added and averaged, followed by subtraction of the CD signal of the solvent. The helix content of the peptides was estimated from the equation:

$$\text{Helix}\ (\%) = (3000 - [\theta]_{222})/39000 \quad (1)$$

where $[\theta]_{222}$ represents the mean residue molar ellipticity at 222 nm [21].

NMR spectroscopy

Three samples, GGN5, ^{PA}GGN5 and ^{CS}GGN5, were prepared from lyophilized peptide to make a 2.5 mM solution in 400 mM SDS-d_{25}/90 % H_2O/10 % ^2H_2O. GGN5^{SH} was prepared by addition of 1 mM DTT-d_{10} to the GGN5 sample. The pH of all the samples was subsequently adjusted to 4.0. Data acquisitions for the homonuclear two-dimensional (2D) double-quantum filtered- (DQF-) COSY, TOCSY and nuclear Overhauser enhancement spectroscopy (NOESY) spectra of all the samples were recorded on Bruker DRX-500 or DRX-600 spectrometers equipped with a gradient unit at 30, 40 and 50 °C, respectively. The 2D TOCSY spectra were acquired using an MLEV-17 spin-lock sequence with isotropic mixing times of 40 and 60 ms, and the NOESY spectra were acquired with mixing times of 150 and 200 ms, respectively. Slowly exchanging amide protons were monitored with a series of 2D NOESY spectra. The first NOESY experiment was started at 20 min after dissolving the lyophilized sample in ^2H_2O, and a series of experiments was recorded at 40, 60, 100, 150, 200, 300 and 600 min. The $^3J_{HNH\alpha}$ coupling constants were measured from the 2D DQF-COSY. All NMR spectra were processed and analysed using the NMRPipe/NMRDraw and NMRView program [22]. Chemical shifts were referenced to methyl signals of sodium 4,4-dimethyl-4-silapentane-1-sulphonate.

Structure calculation

Distance restraints of all the peptides were obtained from the homonuclear 2D NOESY spectra with 200 ms mixing times. Comparisons were made with the NOESY spectra of all the peptides with 150 ms mixing times to assess possible contributions from spin diffusion, which was negligible for a mixing time of 200 ms. All nuclear Overhauser effect (NOE) data were classified into three classes, strong, medium and weak, corresponding to upper-boundary inter-proton distance restraints of 3.0, 4.0 and 5.0 Å, respectively. Lower distance boundaries were taken as the sum of the van der Waals radii of 1.8 Å. Pseudoatom corrections were made for unresolved methyl, methylene and Phe aromatic protons [23]. To generate the structures of GGN5, GGN5^{SH}, ^{PA}GGN5 and ^{CS}GGN5, a total of 324, 316, 351 and 377 NOE constraints were used, respectively. Other restraints for the structure calculations of each peptide such as backbone dihedral

Table 2 Structural statistics of GGN5 and its analogues

vdW, van der Waals.

Restraints for structure calculation	GGN5	GGN5^{SH}	^{PA}GGN5	^{CS}GGN5
Total NOE restraints	324	316	351	377
Intra-residue	84	84	86	88
Sequential ($\|i-j\| = 1$)	108	109	95	132
Medium range ($1 < \|i-j\| < 5$)	102	96	142	13
Long range ($\|i-j\| > 4$)	4	1	4	0
Hydrogen-bond restraints*	26	26	24	24
Dihedral angle restraints†	13	10	15	12
Statistics for structure calculations				
RMSD from idealized covalent geometry				
Bonds (Å)	0.0011 ± 0.0001	0.0012 ± 0.0001	0.0023 ± 0.0001	0.0013 ± 0.0001
Bond angles (°)	0.474 ± 0.003	0.475 ± 0.004	0.468 ± 0.005	0.487 ± 0.003
Improper torsions (°)	0.368 ± 0.005	0.371 ± 0.007	0.373 ± 0.005	0.401 ± 0.004
RMSD from experimental restraints				
Distances (Å)	0.003 ± 0.001	0.003 ± 0.002	0.007 ± 0.002	0.008 ± 0.001
Final energies (kcal/mol)				
E_{total}	31.6 ± 1.9	31.3 ± 1.9	32.3 ± 1.5	35.6 ± 0.9
E_{bonds}	0.5 ± 0.1	0.5 ± 0.1	1.9 ± 0.2	0.7 ± 0.1
E_{angles}	24.5 ± 0.3	24.6 ± 0.5	23.5 ± 0.5	25.9 ± 0.3
$E_{impropers}$	3.8 ± 0.1	3.9 ± 0.2	3.8 ± 0.1	4.5 ± 0.1
E_{vdW}	2.5 ± 1.4	2.0 ± 1.4	2.0 ± 1.4	3.1 ± 0.9
E_{NOE}	0.2 ± 0.2	0.2 ± 0.4	0.9 ± 0.4	1.4 ± 0.3
Average RMSD to the mean structure for the backbone/for non-H atoms (Å)				
Whole (residues 2–24)	0.96/1.51	1.26/1.87	0.80/1.36	1.35/2.07
Helical region (residues 3–20 or 3–19)‡	0.62/1.13	0.60/1.05	0.45/0.95	0.40/0.93
N-terminal region (residues 3–13)	0.35/0.96	0.30/0.90	0.21/0.81	0.18/0.82
C-terminal region (residues 14–20)	0.18/0.81	0.18/0.69	0.24/0.74	0.25/0.79
Disulphide bridge (residues 18–24)§	0.52/1.24	0.90/1.73	0.57/1.27	1.40/2.65

* HN-O, 1.8–2.2 Å; N-O, 2.7–3.3 Å.
† Target angle of $-65 \pm 30°$ for below 6.0 Hz and of $-65 \pm 40°$ for below 6.5 Hz.
‡ In GGN5^{SH} and ^{CS}GGN5, helical region is from residues 3–19.
§ In GGN5^{SH} and ^{CS}GGN5, residues 18–24 are not a disulphide-bridged region.

angle restraints and hydrogen-bond restraints are summarized in Table 2. The backbone dihedral angle restraints were inferred from the $^3J_{HNH\alpha}$ coupling constants and the hydrogen-bond restraints were determined on the basis of the slowly exchanging amide protons and the pattern of the NOEs characteristic of an α-helix. In the case of the GGN5 and ^{PA}GGN5 analogue structures, three additional restraints were added to define the disulphide bridge between Cys-18 and Cys-24. The target values of S-18–S-24, S-18–C_β-24 and S-24–C_β-18 were set to 2.20 ± 0.02, 2.99 ± 0.5 and 2.99 ± 0.5 Å, respectively [24].

The structure calculations of the peptides were performed using repeated iterative cycles of *ab initio* simulated annealing using the force field adapted for NMR structure determination (parallhdg.pro) in XPLOR 3.851 [25]. The simulated annealing was performed from an extended conformation for 30 ps (time step = 5 fs) with an initial annealing temperature of 1000 K, which was followed by 15 ps (time step = 5 fs) cooling step to 100 K. Refinement of the structures was performed using the conjugate gradient Powell algorithm with an initial annealing temperature of 300 K and 5000 cycles of energy minimization, using the same force field file (parallhdg.pro) with *ab initio* simulated annealing protocol. Of the 50 structures that were generated, 45–49 structures of the peptides with no distance violation larger than 0.5 Å and no dihedral violation larger than 5° were accepted. The 20 best structures of the peptides on the basis of their total energy with no systematic distance violation larger than 0.3 Å and no dihedral angle violation larger than 3° were selected as the final structures of the peptides.

Spin label and Mn^{2+} titration experiments

To determine the location of the GGN5 in SDS micelles, the effect of 5- and 12-doxyl stearic acids and Mn^{2+} ions on the proton signal of GGN5 was investigated. The NMR samples were prepared by dissolving GGN5 at 2.5 mM in 400 mM SDS-d_{25} solution in $H_2O/^2H_2O$ (9:1, v/v). After recording the TOCSY spectrum in the absence of the spin-labelled acids and Mn^{2+} ions, 3 μl of the 5- and 12-doxyl stearic acids solubilized in methanol-d_4 were added to the samples to yield a 60:1 molar ratio of detergent corresponding to one spin label per micelle, and the TOCSY spectra were recorded. $MnCl_2$ was dissolved in water before it was added to the sample. Experiments were performed with 1 mM $MnCl_2$. The effects of the 5- and 12-doxyl stearic acids and Mn^{2+} ions were measured by comparing the intensities of the TOCSY cross-peaks in the presence and absence of the spin-labelled acids and/or Mn^{2+} ions. The pH was adjusted to 4.0 and the temperature was 40 °C in all experiments.

RESULTS

Anti-microbial and haemolytic activity

The inhibitory concentrations of GGN5 and its analogues (see Table 1) for various bacteria were summarized in Table 3. The anti-microbial and haemolytic activities of synthetic GGN5 were in good agreement with those of native GGN5 reported previously [10]. GGN5 was more effective against Gram-positive bacteria than against Gram-negative bacteria and was especially

Table 3 Anti-microbial and haemolytic activities of GGN5 and its analogues

Minimal inhibitory concentration was tested three times and a maximal value was selected. Haemolysis (%) is defined to the relative value to 100% haemolysis on human red blood cells (100 μg/ml) treated with 0.2% Triton X-100.

	Minimal inhibitory concentration (μM)			
	GGN5	GGN5^{SH}	^{PA}GGN5	^{CS}GGN5
Micro-organism				
Bacillus subtilis (ATCC 6633)	2.4	2.4	2.5	5.0
Micrococcus luteus (ATCC 10240)	2.4	2.4	2.5	5.0
Staphylococcus aureus (ATCC 6538p)	1.2	2.4	2.5	5.0
Staphylococcus epidermidis (ATCC 12228)	4.8	4.8	4.9	19.8
Escherichia coli (ATCC 25922)	4.8	4.8	4.9	19.8
Shigella dysentariae (ATCC 9752)	19.6	19.6	19.8	> 79.4
Salmonella typhimurium (ATCC 14028)	39.2	39.2	39.6	> 79.4
Citrobacter freundii (ATCC 6750)	19.6	19.6	19.8	79.4
Klebsiella pneumoniae (ATCC 10031)	9.8	9.8	9.9	79.4
Serratia marcescens (ATCC 27117)	> 78.4	> 78.4	> 79.2	> 79.4
Proteus mirabilis (ATCC 25933)	> 78.4	> 78.4	> 79.2	> 79.4
Psuedomonas aeruginosa (ATCC 27853)	78.4	> 78.4	19.8	> 79.4
Haemolysis (%)	6.8	7.5	111.1	1.3

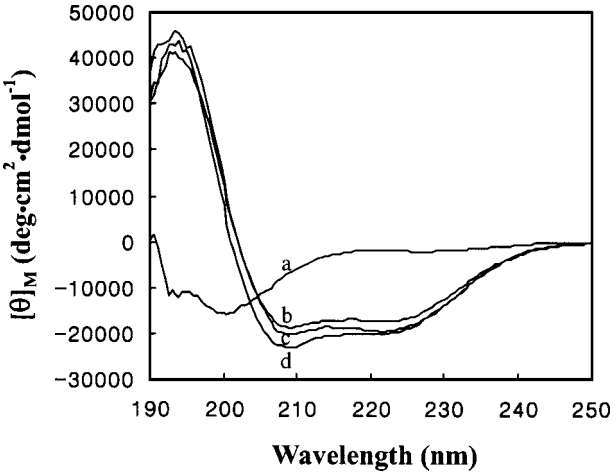

Figure 1 CD spectra of GGN5 in various conditions

Spectra were recorded in (trace a) aqueous buffer, (trace b) 10 mM SDS micelles, (trace c) 5 mM DPC micelles and (trace d) 50% TFE solution. The concentration and the pH of GGN5 were 50 μM and 6.0, respectively. $[\theta]_M$ represents the mean residue molar ellipticity, where M signifies the mean value.

inhibitory to *Staphylococcus*, *Micrococcus* and *Bacillus*. Gram-negative bacteria showed different sensitivity to GGN5 in accordance with each bacterial species. Neither the reduction of a disulphide bridge of GGN5 by the addition of 1 mM dithiothreitol nor replacement of Pro-14 with Ala affected the anti-microbial activity significantly. The anti-microbial activities and specificities of GGN5^{SH} and ^{PA}GGN5 were almost equal to those of GGN5 except in three bacterial strains, *Shigella dysentariae*, *Staphyloccocus aureus* and *Psuedomonas aeruginosa*. In contrast, the anti-microbial activity of ^{CS}GGN5 decreased substantially by 2–8 times compared with that of GGN5 and was almost inactive against Gram-negative bacteria.

In a conventional haemolytic assay on human red blood cells, GGN5 and GGN5^{SH} did not cause significant haemolysis. However, the haemolytic activity of ^{PA}GGN5 increased significantly, but that of ^{CS}GGN5 decreased slightly compared with that of GGN5 (Table 3).

Table 4 Estimated helix contents of GGN5 and its analogues in 50% TFE, 10 mM SDS micelles and 5 mM DPC micelles

Helix content was estimated from eqn. (1) as shown in the Experimental section.

	Helix content (%)		
Peptide	50% TFE	10 mM SDS micelles	5 mM DPC micelles
GGN5	59	52	58
GGN5^{SH}	57	51	57
^{PA}GGN5	67	57	64
^{CS}GGN5	46	45	44

Secondary-structure estimation by CD

The conformational behaviour of GGN5 and its analogues in aqueous buffer, TFE/water solution, SDS micelles and DPC micelles was investigated by using CD. The CD spectra of GGN5 and its analogues recorded in aqueous buffer showed a strong negative band and a weak broad band around 222 nm, indicating a predominantly random coil conformation with a slight helical propensity [26,27]. However, in the presence of membrane mimetics such as TFE/water solution, SDS micelles and DPC micelles, the CD spectra of GGN5 showed two minima at 208 and 222 nm and a cross-over point at about 200 nm, which are characteristics of the presence of a typical α-helical conformation (Figure 1). The helix content of these peptides increased upon increasing either TFE or detergent concentration, and then maximal helix content was reached at 50% TFE/water, 10 mM SDS micelles and 5 mM DPC micelles, respectively. The CD spectra of the analogues of GGN5 also shared a similar pattern with those of GGN5. In addition, there was no significant difference between the CD spectra of all peptides recorded at pH 6.0 and 4.0 under all conditions tested (results not shown).

The helix contents of GGN5 in 50% TFE/water solution, 10 mM SDS micelles and 5 mM DPC micelles were estimated to be about 59, 52 and 58%, respectively (Table 4). The CD spectra of GGN5^{SH} in TFE/water mixture, SDS micelles and DPC micelles indicated that the overall secondary structure of GGN4 was not affected by the addition of dithiothreitol (results not shown). The estimated helix content of GGN5^{SH} was almost equal to that of GGN5. However, the helix content of ^{PA}GGN5 increased by about 5% and that of ^{CS}GGN5 decreased slightly by about 10% compared with that of GGN5 under all conditions tested (Table 4).

NMR assignments and secondary structure determination

The NMR spectra of the peptides were better resolved at 40 °C than at 30 or 50 °C, so most of the spectra were acquired at 40 °C. The assignment of backbone atoms was performed by the standard method proposed by Wüthrich [28]. The proton spin systems were assigned to each amino acid type from the DQF-COSY and TOCSY spectra and were connected in a sequential manner through NOE connectivities shown in Figure 2. The assignment ambiguities due to peak overlaps were resolved by using the spectra recorded at 30 or 50 °C, and by comparing the spectra of each peptide. In particular, the overlapped NH-H_α cross-peaks of Phe-6/Leu-13 and Lys-11/Ser-15 in the spectra of GGN5 were clearly resolved in the spectra of ^{PA}GGN5; therefore the resonance assignment could be performed clearly. Additional

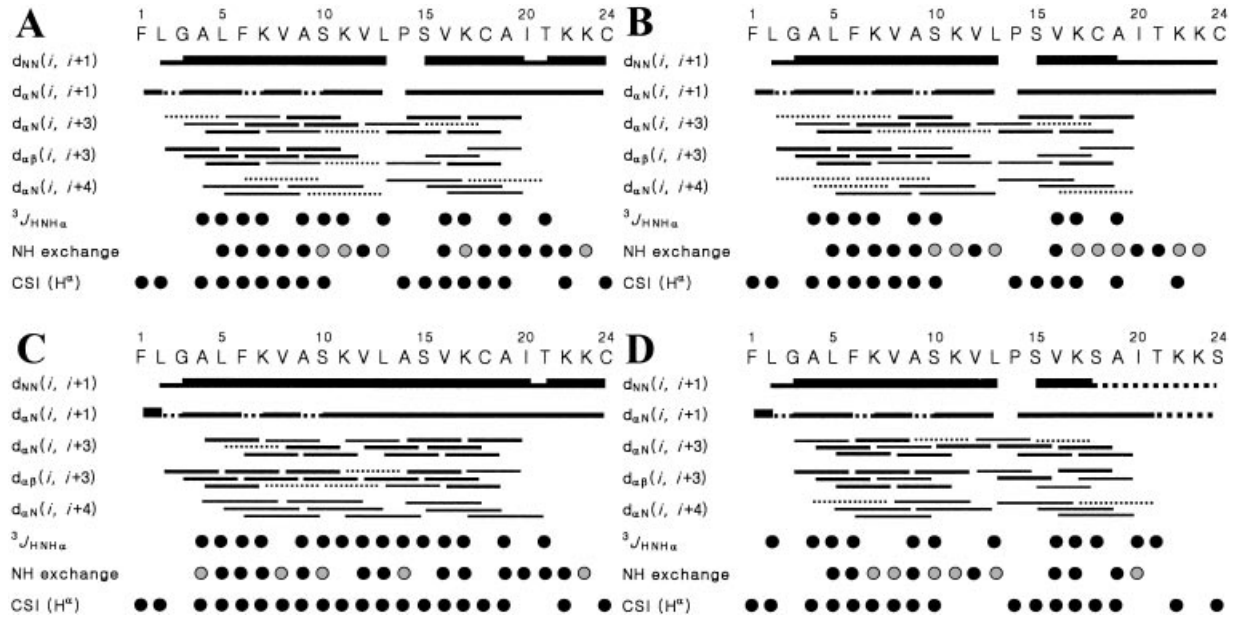

Figure 2 Overview of NMR data for secondary-structure determination

NOE connectivities, $^{3}J_{HNH\alpha}$ coupling constants, amide proton-exchange rates and chemical shift index (CSI) of (**A**) GGN5, (**B**) GGN5^{SH}, (**C**) ^{PA}GGN5 and (**D**) ^{CS}GGN5. The small coupling constants (< 6.5 Hz) and a chemical shift index of -1 are represented as filled circles. Slowly and moderately exchanging amides are represented as black and grey circles, respectively.

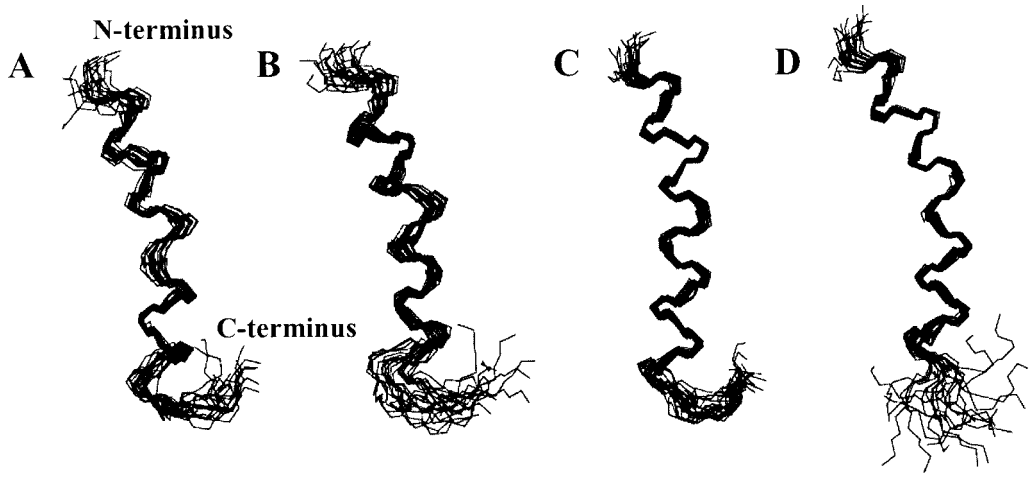

Figure 3 Ensemble of the 20 structures

Backbone atoms of (**A**) GGN5, (**B**) GGN5^{SH}, (**C**) ^{PA}GGN5 and (**D**) ^{CS}GGN5 are superimposed. The structures were calculated from NMR-derived constraints measured in the presence of 400 mM SDS micelles. Residues 3–20 were overlaid in GGN5 and ^{PA}GGN5, while it was residues 3–19 in GGN5^{SH} and ^{CS}GGN5.

NOEs between Leu-13HN, H_{β} and Pro-14H_{δ}, H_{δ}' were used for complete sequential assignment of all three Pro-containing peptides (GGN5, GGN5^{SH} and ^{CS}GGN5). Strong NOE connectivities were observed between Leu-13H_{α} and Pro-14H_{δ} in these Pro-containing peptides, indicative of a *trans* form of the proline [28].

The short and medium inter-residue NOE connectivities of GGN5 and its analogues were same on the whole, except the NOE connectivities around the region substituted by each amino acid. It revealed the nearly complete sets of d_{NN} (i, $i+1$), $d_{\alpha\beta}$ (i, $i+3$), $d_{\alpha N}$ (i, $i+4$) and $d_{\alpha N}$ (i, $i+3$) NOE connectivities for residues 3–20, indicating the presence of regular α-helical conformation. $^{3}J_{HNH\alpha}$ coupling constants of residues 4–20 of all the peptides were less than 6.5 Hz overall except for the following residues: Val-8 and Cys-18 showed about 8.0 Hz, and the residues located around Pro-14 (Val-12, Ser-15 and/or Lys-11 and Leu-13) showed $^{3}J_{HNH\alpha}$ coupling constants of greater than 7.5 Hz (Figure 2). The α-proton chemical shifts of residues 1–19, except residues 11–13, in the Pro-containing peptides showed an overall upfield shift tendency by 0.1–0.5 p.p.m. as compared with the random coil chemical shifts, which also supports the helical conformation of the peptides [29].

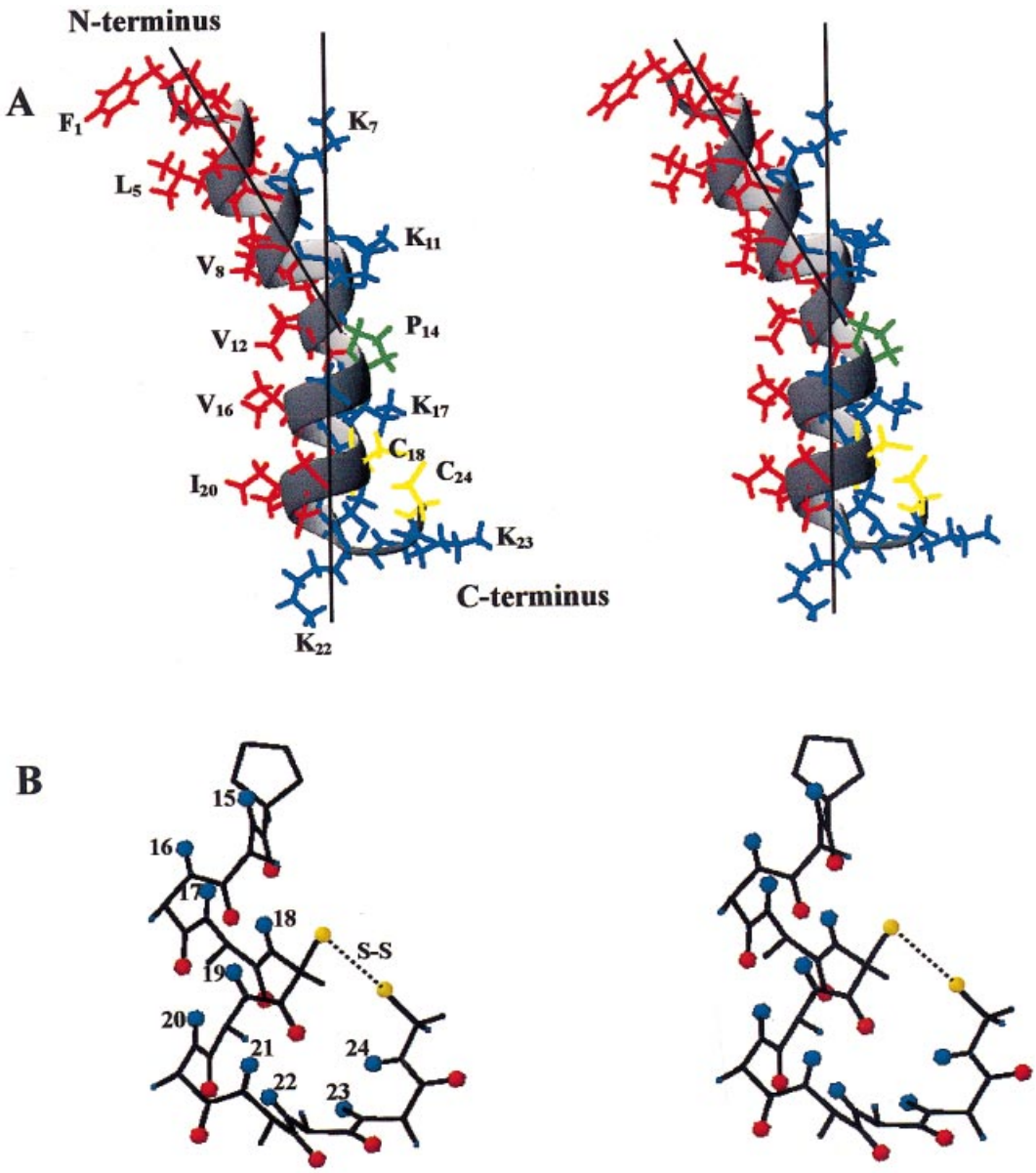

Figure 4 Stereo views of the average structure of GGN5

(**A**) Backbone structure of GGN5 is displayed as a ribbon model, where the hydrophilic and hydrophobic side chains are coloured in blue and red, respectively. The Pro residue is coloured in green and Cys residues are in yellow. A localized distortion of the helical structure is seen. The average kink angle by Pro is $25 \pm 5°$. (**B**) The C-terminal region of GGN5 from residues 14 to 24 is displayed. The amide protons are labelled by residue number and are coloured blue. The atoms of oxygen and sulphur are coloured red and yellow, respectively.

In the case of GGN5 and ^{PA}GGN5, the intra-residue disulphide bond between Cys-18 and Cys-24 could be inferred from the presence of NOE cross-peaks of Cys-18H_β–Cys-24H_β, Cys-18NH–Cys-24H_β and Cys-18H_β–Cys-24HN. It is noteworthy that the chemical shifts of the residues around the C-terminus in GGN5^{SH} were nearly identical with those in GGN5 (results not shown), implying that the local conformation of the C-terminus in GGN5 was not severely affected despite the reduction of a disulphide bridge.

Amide proton exchange

The amide proton-exchange data were analysed semi-quantitatively with each residue in the peptides as exchanging rapidly, moderately or slowly (Figure 2). The amide protons of the residues undergoing complete exchange within 1 h were classified as rapidly exchanging, and those of residues remaining for 10 h of exchange were classified as slowly exchanging. All other residues were classified as moderately exchanging.

Moderately and slowly exchanging amide protons were observed in the central and C-terminal residues of the helical segments spanning residues 6–20 except Ser-15, supporting the hydrogen bonding in helical regions spanning residues 2–20. In contrast, the amide proton of Ala-14 in ^{PA}GGN5 was exchanged moderately, suggesting that ^{PA}GGN5 adopts a more stable α-helical conformation through an additional hydrogen bond between the carbonyl oxygen of Ser-10 and the amide proton of Ala-14, compared with GGN5.

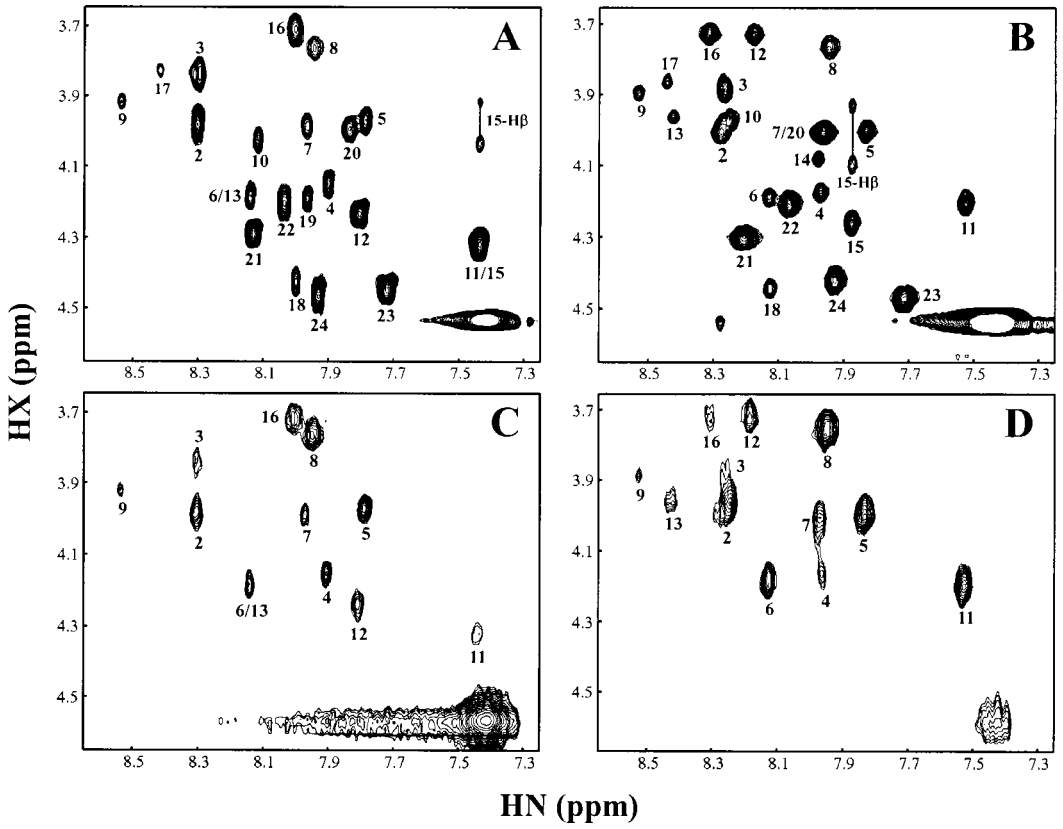

Figure 5 Comparison of NH-H_α regions in TOCSY spectra

TOCSY spectra were recorded in 400 mM SDS micelles: GGN5 in the absence (**A**) and presence (**C**) of $MnCl_2$, ^{PA}GGN5 in the absence (**B**) and presence (**D**) of $MnCl_2$. In (**C**) and (**D**) resonances that were not affected by the presence of $MnCl_2$ are indicated by residue number. HN indicates amide protons and HX indicates alpha or beta protons.

The residues in the C-terminal region from Thr-21 to Lys-23 in GGN5 and ^{PA}GGN5, which does not have helical structure, showed characteristically slow or moderate NH exchange rates (Figures 2A and 2C). Accordingly, it seems that these amides are located in the hydrophobic environment created by the Cys-18–Cys-24 disulphide bridge. In GGN5^{SH} the amide proton of Thr-21 was also slowly exchanged, and therefore a loop-like conformation in the C-terminal region seems to be maintained despite the absence of the disulphide bridge. However, the amide protons of the C-terminal residues in GGN5^{CS} were exchanged rapidly, indicating that the C-terminal region does not have an ordered conformation.

Except for the C-terminal residues, it is noteworthy that very slowly exchanging residues of Leu-5, Phe-6, Val-8, Ala-9, Val-12 and Val-16 are all hydrophobic residues, suggesting that these residues are shielded from the water in the bulk solution through the hydrophobic interaction with micelles and/or they are involved in the inter-residue hydrogen bonding.

Three-dimensional structure

Simulated annealing calculations were run to produce a set of 50 structures of GGN5, GGN5^{SH}, ^{PA}GGN5 and ^{CS}GGN5 with a common fold that were in good agreement with the experimental restraints and had low total energies. Out of 50 structures of the peptides, 45–49 structures with no distance violation larger than 0.5 Å and no dihedral violation larger than 5° were accepted. Then the 20 structures with the lowest energies and no distance violation larger than 0.3 Å and no dihedral violation larger than 3° were selected to represent the solution structures of the peptides in SDS micelles.

The 20 converged structures of GGN5 shown in Figure 3(A) have a well-defined α-helix spanning residues 3–20. A Pro-14 residue produces a break in the hydrogen bond of an amide proton of the following residue Ser-15 to the carbonyl oxygen of Lys-11 and induces a kink with an angle of $25 \pm 5°$. The helical region shows a typical amphipathic character, in which the hydrophobic residues are located on the concave side of helix created by a helical kink, while the hydrophilic residues are located on the convex side of the helix (Figure 4A). The 20 final converged structures of GGN5 exhibited a root-mean-square deviation (RMSD) about the mean co-ordinate position for residues 3–20 of 0.62 Å for the backbone atoms (N, Cα, C′) and 1.51 Å for all heavy atoms. The C-terminal region of GGN5 reveals a well-defined loop-like conformation through the intra-residue disulphide bridge between Cys-18 and Cys-24. The average RMSD value of this loop region was 0.52 Å for the backbone atoms. As shown in Figure 4(B), all the amide protons of residues 20–24 are located in the hydrophobic interior of the disulphide-bridged loop.

Figure 3(B) shows that the overall structure of GGN5^{SH} is similar to that of GGN5 except for the local conformation of the C-terminus. The stable helix is slightly shortened to residues 3–19, probably due to the reduction of the disulphide bridge. However,

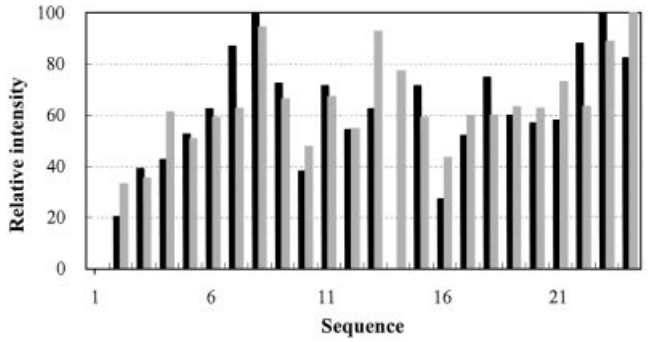

Figure 6 Comparison of NMR signal intensities

The ratio of signal intensities from TOCSY spectra of GGN5 or ^{PA}GGN5 in the presence of 5-doxyl stearic acid to those from a reference spectrum without 5-doxyl stearic acid is indicated. 5-Doxyl stearic acid was added at a concentration of 1 spin label/SDS micelle. Black bars, GGN5; grey bars, ^{PA}GGN5.

the C-terminal loop-like conformation seems to be maintained despite the reduction of the disulphide bridge, which may explain the slow exchange of the amide proton of Thr-21 (Figure 2B). The average RMSD value of residues 18–24 was 0.9 Å for the backbone atoms, indicative of loosely defined conformation.

^{PA}GGN5 adopts a straight α-helical structure in the central region by replacing the residue of Pro-14 with Ala, while a localized bending of its helical structure is still shown around the Val-8 residue by the angle of about 5–10° (Figure 3C). An additional hydrogen bond between an amide proton of Ala-14 and a carbonyl oxygen of Ser-10, which could be inferred from moderate exchange of Ala-14 amide proton, will stabilize the central helical structure. The α-proton chemical shifts of Lys-11, Val-12, Leu-13 and Ser-15 residues in ^{PA}GGN5 were shifted to upfield as compared with that of GGN5, also indicating that the central helical structure of ^{PA}GGN5 is more stable than that of GGN5. The 20 final converged structures of ^{PA}GGN5 exhibited RMSDs for residues 3–20 of 0.45 Å for the backbone atoms and of 0.95 Å for all heavy atoms, which is also smaller than that of GGN5.

In ^{CS}GGN5, although its structure in the helical region is similar to that of GGN5, the C-terminal region of residues 20–24 shows a completely disordered conformation (Figure 3D). The disordered conformation will reduce the overall helical stability to lead to a decrease in CD intensity, overall amphipathicity and hydrophobicity of ^{CS}GGN5 compared with GGN5.

Location of the peptides in SDS micelles

Figure 5 shows the 2D TOCSY fingerprint region of GGN5 and ^{PA}GGN5 bound to SDS micelles in the absence and presence of Mn^{2+} ions. On addition of Mn^{2+} ions, mainly the HN-H_α cross-peaks of the residues in the C-terminal region of both peptides disappeared or weakened remarkably, due to the severe peak broadening. In contrast, the N-terminal and central residues of GGN5, especially the hydrophobic residues of Leu-2, Gly-3, Ala-4, Leu-5, Phe-6, Val-8, Ala-9, Val-12, Leu-13 and Val-16, were hardly affected at all, and the hydrophilic residues of Lys-7, Lys-11 and Ser-15 were slightly affected (Figure 5C). In the case of ^{PA}GGN5, the residues affected by the presence of Mn^{2+} were almost similar to those of GGN5 except for some residues. On addition of Mn^{2+}, C-terminal residues from Ala-14 to Cys-24 were the most affected, while Leu-5, Phe-6, Val-8 and Lys-11 were hardly affected and residues Leu-2, Gly-3, Ala-4, Lys-7, Ala-9, Ser-10, Lys-11, Val-12 and Leu-13 were slightly affected (Figure 5D).

The presence of 5-doxyl stearic acid reduced significantly the resonance intensities of the hydrophobic residues of GGN5 located mainly in the N-terminal region except Val-8, while the intensities of the hydrophilic residues except Ser-10 were slightly affected (Figure 6). The cross-peaks of the side chains in hydrophobic residues were more affected than the HN-H_α cross-peaks, and the six consecutive hydrophobic residues of N-terminus from Phe-1 to Phe-6 were most affected by the presence of 5-doxyl stearic acid. However, all signal intensities remained constant after addition of 1 molecule of 12-doxyl stearic acid/micelle, thereby proving that no residues of GGN5 became embedded in the hydrophobic core of the micelle (results not shown). In $GGN5^{PA}$, 5-doxyl stearic acid had a large effect on the residues of Leu-2, Gly-3, Leu-5, Ser-10, Val-12 and Val-16. Several hydrophobic residues, Leu-2, Ala-4, Leu-13 and Val-16, were less affected, while several hydrophilic residues, Lys-7, Ser-15, Lys-22 and Lys-23 were more affected than those of GGN5 (Figure 6).

DISCUSSION

Most anti-microbial peptides isolated from the *Rana* genus share a characteristic intra-residue disulphide bridge of heptapeptide motif in their C-terminus and highly conserved amino acids [1]. Though several structures of these peptides were determined and characterized functionally [11–14,30], the precise roles of the conserved sequence and the disulphide bridge in the structure and activity have not been elucidated yet. We therefore investigated the role of Pro and Cys residues, the highly conserved amino acids, and the disulphide bridge in the structure and activity of GGN5.

GGN5 and its analogues that we have tested showed their respective anti-microbial and haemolytic activities. The anti-microbial activity and sensitivity of GGN5 on various bacteria were hardly affected by reducing the disulphide bridge. Similar results have been reported that the activities of other anti-microbial peptides such as brevinin 1E [30] and GGN4 [11] were not affected by the addition of 1–10 mM dithiothreitol as a strong reducing agent. On the other hand, replacement of both Cys-18 and Cys-24 with Ser residues in GGN5 decreased considerably both the anti-microbial and haemolytic activities. Therefore, it could be thought that the disulphide bridge does not have important roles in the anti-microbial activity of GGN5, but that Cys-18 and Cys-24 themselves do. By replacing a Pro-14 with an Ala, the anti-microbial activity increased slightly, while the haemolytic activity increased significantly. These results imply that a helical kink by the Pro-14 residue is crucial for the haemolytic activity of GGN5.

Primary and secondary structure of the peptides

It is well known that the properties such as net charge, hydrophobicity and hydrophobic moment are important for the activity in the anti-microbial peptides adopting an α-helical structure [31–34]. GGN5 is a cationic peptide carrying five Lys residues. The hydrophobicity ($\langle H \rangle$) and hydrophobic moment ($\langle \mu_H \rangle$) values of GGN5 for the helical region spanning residues 3–20 are 0.32 and 0.43 respectively, by the method of Eisenberg et al. [35]. The three analogues of GGN5, ^{PA}GGN5 ($\langle H \rangle = 0.35$, $\langle \mu_H \rangle = 0.40$), $GGN5^{SH}$ ($\langle H \rangle = 0.26$, $\langle \mu_H \rangle = 0.40$) and ^{CS}GGN5 ($\langle H \rangle = 0.23$, $\langle \mu_H \rangle = 0.42$), exhibited similar hydrophobic moments, but lower hydrophobicities were shown in $GGN5^{SH}$ and ^{CS}GGN5 compared with GGN5, which is mainly due to a decrease in the helical length from 3 to 19 in $GGN5^{SH}$ and ^{CS}GGN5.

The estimated helical contents of the peptides were slightly different, in the order of ^{PA}GGN5 > GGN5 > GGN^{SH} > ^{CS}GGN5. Notably, the magnitude of the anti-microbial activity of the peptides is also arranged in the order of ^{PA}GGN5 ⩾ GGN5 ⩾ GGN5^{SH} > ^{CS}GGN5, suggesting that the helical content of the peptides is an important factor for the anti-microbial activity of GGN5.

Structure–activity relationship of GGN5

Since it is difficult to determine the structure of peptides in the membrane-bound state, NMR studies of GGN5 and its analogues were performed in deuterated SDS micellar solution. It was previously shown that this membrane mimetic induces a similar conformational change as binding to the membrane [36].

GGN5 adopts a rod-like α-helical conformation which has a kink around Pro-14 with a bend angle of $25 \pm 5°$, as shown in Figure 3(A). The kink is associated with high $^3J_{HN\alpha H}$ coupling constants in the sequence of Val-12 and Ser-15. The break of the chemical shift index ('CSI') from residues Lys-11 to Leu-13 also indicates the kink conformation around Pro-14. However, the NOE connectivities, $d_{\alpha N}$ (i, $i+3$) of Val-12–Ser-15 and Leu-13–Val-16, and $d_{\alpha N}$ (i, $i+4$) of Leu-13–Lys-17, were observed, indicating the existence of a regular helical conformation despite the kink. Slowly or moderately exchanged amide protons around Pro-14 except Ser-15 also support the helical conformation around the kink through the hydrogen bond. The C-terminus of GGN5 adopts a loop-like conformation by an intra-residue disulphide bridge between Cys-18 and Cys-24. Although the NOE between the H_α of one Cys residue and the H_β of the other one in the disulphide bridge was not identified, due to the overlap of the α-proton resonances of the two Cys residues, the presence of NOE connectivities of Cys-18H_β–Cys24H_β, Cys-18NH–Cys-24H_β and Cys-18H_β–Cys-24HN allows us to identify the intra-residue disulphide bridge. The amide protons of GGN5 from residues Thr-21 to Cys-24 are located in the hydrophobic interior formed by the loop-like structure, and as a result they exchange very slowly (Figure 4B).

Despite the reduction of the disulphide bridge, the overall structure of GGN5^{SH} is similar to that of GGN5 and the loop-like conformation of C-terminus is also maintained, albeit loosely ordered compared with GGN5. The possibility of oxidization of the sample during the experimental process could be excluded, since we have verified that 1 mM dithiothreitol is sufficient to reduce the disulphide bridge of GGN4, one of the anti-microbial peptides in the GGN family [11]. Accordingly, structural similarity between GGN5^{SH} and GGN5, despite the presence or absence of the disulphide bridge, will give rise to only a small difference in the amide proton exchanges, the chemical shift values and the anti-microbial activities between them. Some other peptides, such as GGN4 and ranalexin, have also shown similar results, i.e. their anti-microbial activities and chemical shifts of α- and side-chain protons are not affected significantly and only the chemical shifts of amide protons and/or ^{15}N around the Cys residues are slightly affected by reduction of the disulphide bridge [11,12].

By replacing Pro-14 with Ala, ^{PA}GGN5 adopts a rigid helix with a slight bend around the Val-8 residue with an angle of about 10°. Other non-proline-containing anti-microbial peptides are often curved, e.g. magainin 2 does not have a central proline residue, but adopts an α-helical structure in DPC with a bend angle of 16° [37]. Nonetheless, the central helical structure of ^{PA}GGN5 is more stabilized and rigid than that of GGN5, probably leading to the increase of the molar ellipticity at 222 nm in CD spectra (results not shown). Since the Ala residue has a strong preference for an α-helix conformation, the helical structures of many anti-microbial peptides containing a proline residue at their central helix region are generally stabilized and made rigid by replacing a Pro with an Ala residue [14–18,20]. The physicochemical properties and activities of these peptides could be also affected significantly by replacement of a Pro with an Ala residue. By replacing a Pro with an Ala, melittin exhibited twice the haemolytic activity, but was less able to induce voltage-dependent ion conductance in planar bilayers [17,18,38]. On the other hand, the anti-microbial activity of buforin II and maculatin 1.1 decreased on replacement of a Pro with an Ala or a Leu, which was due to the decrease of the cell-penetrating efficiency of buforin II [15,16] or the decrease of the ability of interaction with the membrane of maculatin 1.1, respectively [39]. Since the hydrophobicity and hydrophobic moment of GGN5 were not much affected by the replacement of a Pro with an Ala residue, it could be thought that the helical flexibility through the kink is the most important factor for the haemolytic activity of GGN5.

Peptides such as tachyplesin [40] and defensins [41] have two or more disulphide bridges and adopt mainly a β-sheet conformation, while GGN5 has one disulphide bridge in its C-terminus. The disulphide bridges in tachyplesin and defensins are crucial to form an overall amphipathic three-dimensional fold and to maintain the anti-microbial activities [42–44]. Replacement of two Cys residues with Ser residues in GGN5 perturbed the hydrophobicity/amphipathicity balance, and induced a disordered conformation in its C-terminus which results in the decrease of its helical length and stability. This result seems to be closely related with the decrease of both anti-microbial and haemolytic activities of ^{CS}GGN5. The appropriate helical stability and length enough to span the lipid bilayer as well as the appropriate proportion of helical hydrophobicity to amphipathicity are important for anti-microbial activity. Consequently, it could be suggested that the disulphide-bonded loop-like conformation of GGN5 in C-terminus stabilizes the helical conformation to allow it fully to exhibit anti-microbial activity.

Interaction of peptides with the membrane mimetic

The orientation of the peptide relative to the SDS micelles was investigated using the paramagnetic probes Mn^{2+}, 5-doxyl stearic acid and 12-doxyl stearic acid. The paramagnetic probes were known to cause the broadening of the residues just outside the micelles (Mn^{2+}), inside but close to the surface of the micelles (5-doxyl) and deeply buried in the micelles (12-doxyl), respectively [45,46]. These probes lead to dramatically accelerated longitudinal and transverse relaxation rates of protons in spatial proximity via highly efficient spin and electron relaxation [47]. This effect depends on the distance between the probes and the protons and is clearly observed as a loss of signal intensity in 2D TOCSY spectra for amide protons or side-chain protons located closely to the spin label.

Addition of spin label to the GGN5 bound to SDS micelles only affects a specific subset of the resonances. The remaining intensity of the resonance shows an inverse relationship with the broadening factor, except for the resonances of a few residues. The resonances that are affected most by Mn^{2+} ions were mainly the C-terminal region from Ser-15 to Cys-24, except Val-16, and hydrophilic residues of Lys-7 and Lys-11 in the N-terminal helical region were slightly affected (Figure 5C). On the other hand, 5-doxyl stearic acid causes a background broadening of the resonances of almost every residue of GGN5 except the C-terminal region and large effects are observed for the hydrophobic

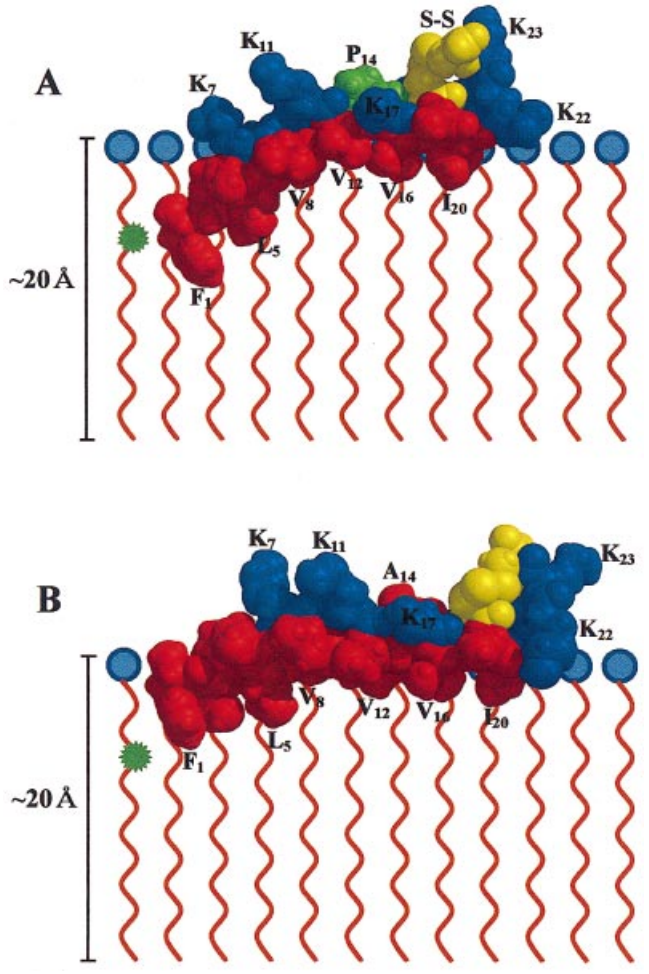

Figure 7 Schematic drawing of GGN5 and ^{PA}GGN5 bound to SDS micelles

(**A**) GGN5. (**B**) ^{PA}GGN5. The position of 5-doxyl stearic acid is indicated by a star. Hydrophobic and hydrophilic residues are represented in red and blue, respectively. Pro and Cys residues are green and yellow, respectively.

residues, especially the hydrophobic cluster of the N-terminal region from Phe-1 to Phe-6 (Figure 6). Since Mn^{2+} ions are located on the surface of the micelles and 5-doxyl stearic acid is just under the surface, the results obtained with the spin-label experiments can be used to interpret the relative orientation of GGN5 to the SDS micelles. The results of spin-label experiments are closely related to amide proton exchange experiments; that is, hydrophobic residues are exchanged slowly, probably due to hydrophobic interaction with SDS micelles as well as intra-residue hydrogen bond in helical structure. Proton–deuterium exchange experiments have long been used to prove that amide protons are involved in hydrogen bonds or are shielded from solvent access to a large extent [48]. Recently, these experiments have also been recognized to detect the residues involved in binding of peptides to membranes. Amide protons from residues at the interface are shielded from solvent and display largely reduced exchange rates [49].

From all these results, we could suggest the following model (Figure 7A). The amphipathic helix of GGN5, extending from residues Gly-3 to Ile-20, is kinked around the Pro-14 residue by a bend angle of about 25°. The helical kink may facilitate and stabilize the diagonal binding of GGN5 to SDS micelles through mainly hydrophobic interaction between hydrophobic residues of GGN5 and head group of SDS micelles. NMR studies have shown that other anti-microbial peptides containing proline and adapting helical structure have a similar bend angle of $30 \pm 10°$ in membrane mimic environments, e.g. melittin in methanol has a kink of 20° between the two helical portions [18], alamethicin in methanol has a central bend ($35 \pm 5°$) [50], buforin II in TFE/water [15] and ranalexin in dodecylphocholine [12] show similar patterns, and maculatin 1.1 in TFE/water has a slight kink and flexibility in its central region [39]. These kinks by proline residues increased overall helical flexibility and amphipathicity and as a result increased the membrane-binding efficiency and/or facilitated the peptides to form an oligomer by channel-stabilizing hydrogen bonds.

On the other hand, the C-terminal helix from residues Ser-15 to Ile-20 may lie parallel on the SDS micelles and interact dynamically with SDS micelles through Val-16, Ala-19 and Ile-20. Since it has been reported that the disulphide-bonded loop of chromogranin B, a secretory protein in neuroendocrine cells, mediates membrane binding [51], we investigated the effect of a disulphide-bonded loop and two lysine residues located in the loop on binding of GGN5 to SDS micelles. As shown from $MnCl_2$ and 5-doxyl stearate titration experiments on GGN5, the residues of the C-terminal disulphide-bonded loop of GGN5 locate mainly on the surface of SDS micelles to interact dynamically with the SDS micelle surface. On the other hand, it seems that two lysine residues in the loop are totally exposed to the solvent, implying that their positively charged side chains may interact with anionic SDS head groups through electrostatic interaction. Since the physicochemical properties of the disulphide-bonded loop are quite different between chromogranin B and GGN5, i.e. the disulphide-bonded loop of chromogranin (22 residues) is much longer and more hydrophobic than that of GGN5, it could be that membrane binding of the disulphide-bonded loop of GGN5 is much weaker than that of chromogranin B.

In ^{PA}GGN5, considering all the results of the structure bound to SDS micelles, the amide proton-exchange rates, and the spin-label experiments, it is shown that the binding angle of the N-terminal region of ^{PA}GGN5 to the SDS micelle surface decreased slightly compared with that of GGN5, but that the overall orientation of ^{PA}GGN5 to SDS micelles was similar to that of GGN5 (Figure 7B). Although the straight helix in the central region of ^{PA}GGN5 was formed by replacing Pro-14 with Ala, a slight bend around Val-8 could face the N-terminal hydrophobic cluster (Phe-1–Phe-6) towards the interior of SDS micelles to bind tightly with the head group of SDS micelles. Other hydrophobic residues (Val-8, Val-12 and Val-16) are also able to interact dynamically with SDS micelles, as GGN5 does. Accordingly, structural similarity on SDS micelles between GGN5 and ^{PA}GGN5 may explain their similar anti-microbial activities, while the kink angle and flexibility in the central helical region of GGN5 may be requisite for discrimination of target cells, as shown by their different haemolytic activities.

^{CS}GGN5 revealed similar results to GGN5 in $MnCl_2$ titration experiments, while we could not analyse clearly the data of 5-doxyl stearate titration experiments on ^{CS}GGN5 due to severe peak overlap (results not shown). According to a rough interpretation of the spectra, Ala-19 and Ile-20 of ^{CS}GGN5 were supposed to be less affected than those of GGN5 by 5-doxyl stearate, suggesting that the C-terminal region of ^{CS}GGN5 binds more weakly than that of GGN5, probably due to the decrease of helical length and stability by the absence of loop conformation.

In conclusion, we have compared the anti-microbial and haemolytic activity and the three-dimensional structure of GGN5 bound to SDS micelles with those of its analogues to investigate the structure–activity relationship of GGN5. Two important structural factors for the activity of GGN5 could be determined from our results. First, the flexible helical kink by a central proline is important for the haemolytic activity of GGN5. Second, the presence of a disulphide-bonded loop-like structure in the C-terminus of GGN5 stabilizes the C-terminal helical structure, which could afford GGN5 the ability to bind stably to the membrane of target cells, leading to the exhibition of full biological activity of the peptide. Assuming that GGN5 acts as an ion channel by forming an oligomer to kill target cells, like other well-known anti-microbial peptides adopting an amphipathic helix, we could suggest that the central helical kink and the C-terminal disulphide-bonded loop-like conformation afford GGN5 maximal amphipathicity, allowing it to form the oligomer.

This research was supported by the National Research Laboratory Program (M1-0203-00-0075) from the Korea Institute Science & Technology Evaluation and Planning, Republic of Korea, and also in part by 2002 BK21 project for Medicine, Dentistry and Pharmacy.

REFERENCES

1 Boman, H. G. (1995) Peptide antibiotics and their role in innate immunity. Annu. Rev. Immunol. **13**, 61–92

2 Nicolas, P. and Mor, A. (1995) Peptides as weapons against microorganisms in the chemical defense system of vertebrates. Annu. Rev. Microbiol. **49**, 277–304

3 Zasloff, M. (1987) Magainins, a class of antimicrobial peptides from *Xenopus* skin: isolation, characterization of two active forms, and partial cDNA sequence of a precursor. Proc. Natl. Acad. Sci. U.S.A. **84**, 5449–5453

4 Morikawa, N., Hagiwara, K. and Nakajima, T. (1992) Brevinin-1 and -2, unique antimicrobial peptides from the skin of the frog, *Rana brevipoda porsa*. Biochem. Biophys. Res. Commun. **189**, 184–190

5 Simmaco, M., Mignogna, G., Barra, D. and Bossa, F. (1993) Novel antimicrobial peptides from skin secretion of the European frog *Rana esculenta*. FEBS Lett. **324**, 159–161

6 Clark, D. P., Durell, S., Maloy, W. L. and Zasloff, M. (1994) Ranalexin. A novel antimicrobial peptide from bullfrog (*Rana catesbeiana*) skin, structurally related to the bacterial antibiotic, polymyxin. J. Biol. Chem. **269**, 10849–10855

7 Mor, A., Nguyen, V. H., Delfour, A., Migliore-Samour, D. and Nicolas, P. (1991) Isolation, amino acid sequence, and synthesis of dermaseptin, a novel antimicrobial peptide of amphibian skin. Biochemistry **30**, 8824–8830

8 Gibson, B. W., Tang, D. Z., Mandrell, R., Kelly, M. and Spindel, E. R. (1991) Bombinin-like peptides with antimicrobial activity from skin secretions of the Asian toad, *Bombina orientalis*. J. Biol. Chem. **266**, 23103–23111

9 Simmaco, M., Barra, D., Chiarini, F., Noviello, L., Melchiorri, P., Kreil, G. and Richter, K. (1991) A family of bombinin-related peptides from the skin of *Bombina variegate*. Eur. J. Biochem. **199**, 217–222

10 Park, J. M., Jung, J. E. and Lee, B. J. (1994) Antimicrobial peptides from the skin of a Korean frog, *Rana rugos*. Biochem. Biophys. Res. Commun. **205**, 948–954

11 Park, S. H., Kim, Y. K., Park, J. W., Lee, B. and Lee, B. J. (2000) Solution structure of the antimicrobial peptide gaegurin 4 by ^{1}H and ^{15}N nuclear magnetic resonance spectroscopy. Eur. J. Biochem. **267**, 2695–2704

12 Vignal, E., Chavanieu, A., Roch, P., Chiche, L., Grassy, G., Calas, B. and Aumelas, A. (1998) Solution structure of the antimicrobial peptide ranalexin and a study of its interaction with perdeuterated dodecylphosphocholine micelles. Eur. J. Biochem. **253**, 221–228

13 Suh, J. Y., Lee, K. H., Chi, S. W., Hong, S. Y., Choi, B. W., Moon, H. M. and Choi, B. S. (1996) Unusually stable helical kink in the antimicrobial peptide – a derivative of gaegurin. FEBS Lett. **392**, 309–312

14 Suh, J. Y., Lee, Y. T., Park, C. B., Lee, K. H., Kim, S. C. and Choi, B. S. (1999) Structural and functional implications of a proline residue in the antimicrobial peptide gaegurin. Eur. J. Biochem. **266**, 665–674

15 Park, C. B., Yi, K. S., Matsuzaki, K., Kim, M. S. and Kim, S. C. (2000) Structure-activity analysis of buforin II, a histone H2A-derived antimicrobial peptide: the proline hinge is responsible for the cell-penetrating ability of buforin II. Proc. Natl. Acad. Sci. U.S.A. **97**, 8245–8250

16 Kobayashi, S., Takeshima, K., Park, C. B., Kim, S. C. and Matsuzaki, K. (2000) Interactions of the novel antimicrobial peptide buforin 2 with lipid bilayers: proline as a translocation promoting factor. Biochemistry **39**, 8648–8654

17 Blondelle, S. E. and Houghten, R. A. (1991) Probing the relationships between the structure and hemolytic activity of melittin with a complete set of leucine substitution analogs. Pept. Res. **4**, 12–18

18 Dempsey, C. E., Bazzo, R., Harvey, T. S., Syperek, I., Boheim, G. and Campbell, I. D. (1991) Contribution of proline-14 to the structure and actions of melittin. FEBS Lett. **281**, 240–244

19 Gazit, E., Boman, A., Boman, H. G. and Shai, Y. (1995) Interaction of the mammalian antibacterial peptide cecropin P1 with phospholipid vesicles. Biochemistry **34**, 11479–11488

20 Dathe, M., Kaduk, C., Tachikawa, E., Melzig, M. F., Wenschuh, H. and Bienert, M. (1998) Proline at position 14 of alamethicin is essential for hemolytic activity, catecholamine secretion from chromaffin cells and enhanced metabolic activity in endothelial cells. Biochim. Biophys. Acta **1370**, 175–183

21 Morrisett, J. D., David, J. S., Pownall, H. J. and Gotto, Jr, A. M. (1973) Interaction of an apolipoprotein (apoLP-alanine) with phosphatidylcholine. Biochemistry **12**, 1290–1299

22 Delaglio, F., Grzesiek, S., Vuister, G., Zhu, G., Pfeifer, J. and Bax, A. (1995) NMRPipe: a multidimensional spectral processing system based on UNIX pipes. J. Biomol. NMR **6**, 277–293

23 Wüthrich, K., Billeter, M. and Braun, W. (1983) Pseudo-structures for the 20 common amino acids for use in studies of protein conformations by measurements of intramolecular proton-proton distance constraints with nuclear magnetic resonance. J. Mol. Biol. **169**, 949–961

24 Nilges, M., Gronenborn, A. M., Brünger, A. T. and Clore, G. M. (1988) Determination of three-dimensional structures of proteins by simulated annealing with interproton distance restraints. Application to crambin, potato carboxypeptidase inhibitor and barley serine proteinase inhibitor 2. Protein Eng. **2**, 27–38

25 Brünger, A. T. (1992) Xplor 3.1. A System for X-ray Crystallography and NMR, Yale University Press, New Haven, CT

26 Wienk, H. L., Czisch, M. and de Kruijff, B. (1999) The structural flexibility of the preferredoxin transit peptide. FEBS Lett. **453**, 318–326

27 Yoon, M. K., Park, S. H., Won, H. S., Na, D. S. and Lee, B. J. (2000) Solution structure and membrane-binding property of the N-terminal tail domain of human annexin I. FEBS Lett. **484**, 241–245

28 Wüthrich, K. (1986) NMR of Proteins and Nucleic Acids, John Wiley and Sons, New York

29 Wishart, D. S., Sykes, B. D. and Richards, F. M. (1992) The chemical shift index: a fast and simple method for the assignment of protein secondary structure through NMR spectroscopy. Biochemistry **31**, 1647–1651

30 Kwon, M. Y., Hong, S. Y. and Lee, K. H. (1998) Structure-activity analysis of brevinin 1E amide, an antimicrobial peptide from *Rana esculenta*. Biochim. Biophys. Acta **1387**, 239–248

31 Lee, S., Mihara, H., Aoyagi, H., Kato, T., Izumiya, N. and Yamazaki, N. (1986) Relationship between antimicrobial activity and amphiphilic property of basic model peptides. Biochim. Biophys. Acta **862**, 211–219

32 Blondelle, S. E. and Houghten, R. A. (1992) Design of model amphipathic peptides having potent antimicrobial activities. Biochemistry **31**, 12688–12694

33 Bessalle, R., Gorea, A., Shalit, I., Metzger, J. W., Dass, C., Desiderio, D. M. and Fridkin, M. (1992) Structure-function studies of amphiphilic antibacterial peptides. J. Med. Chem. **36**, 1203–1209

34 Pathak, N., Salas-Auvert, R., Ruche, G., Janna, M. H., McCarthy, D. and Harrison, R. G. (1995) Comparison of the effects of hydrophobicity, amphiphilicity, and α-helicity on the activities of antimicrobial peptides. Proteins **22**, 182–186

35 Eisenberg, D., Schwarz, E., Komaromy, M. and Wall, R. (1984) Analysis of membrane and surface protein sequences with the hydrophobic moment plot. J. Mol. Biol. **179**, 125–142

36 Beinert, D., Neumann, L., Uebel, S. and Tampe, R. (1997) Structure of the viral TAP-inhibitor ICP47 induced by membrane association. Biochemistry **36**, 4694–4700

37 Gesell, J., Zasloff, M. and Opella, S. J. (1997) Two-dimensional ^{1}H NMR experiments show that the 23-residue magainin antibiotic peptide is an α-helix in dodecylphosphocholine micelles, sodium dodecylsulfate micelles and trifluorethanol/water solution. J. Biomol. NMR **9**, 127–135

38 Rex, S. (2000) A Pro→Ala substitution in melittin affects self-association, membrane binding and pore-formation kinetics due to changes in structural and electrostatic properties. Biophys. Chem. **85**, 209–228

39 Chia, B. C., Carver, J. A., Mulhern, T. D. and Bowie, J. H. (2000) Maculatin 1.1, an anti-microbial peptide from the Australian tree frog, *Litoria genimaculata* solution structure and biological activity. Eur. J. Biochem. **267**, 1894–1908

40 Kawano, K., Yoneya, T., Miyata, T., Yoshikawa, K., Tokunaga, F., Terada, Y. and Iwanaga, S. (1990) Antimicrobial peptide, tachyplesin I, isolated from hemocytes of the horseshoe crab (*Tachypleus tridentatus*). NMR determination of the beta-sheet structure. J. Biol. Chem. **265**, 15365–15367

41 Kagan, B. L., Ganz, T. and Lehrer, R. I. (1994) Defensins: a family of antimicrobial and cytotoxic peptides. Toxicology **87**, 131–149

42 Matsuzaki, K., Nakayama, M., Fukui, M., Otaka, A., Funakoshi, S., Fujii, N., Bessho, K. and Miyajima, K. (1993) Role of disulfide linkages in tachyplesin-lipid interactions. Biochemistry **32**, 11704–11710
43 Matsuzaki, K., Yoneyama, S., Fujii, N., Miyajima, K., Yamada, K., Kirino, Y. and Anzai, K. (1997) Membrane permeabilization mechanisms of a cyclic antimicrobial peptide, tachyplesin I, and its linear analog. Biochemistry **36**, 9799–9806
44 White, S. H., Wimley, W. C. and Selsted, M. E. (1995) Structure, function, and membrane integration of defensins. Curr. Opin. Struct. Biol. **4**, 521–527
45 Papavoine, C. H., Konings, R. N., Hilbers, C. W. and van de Ven, F. J. (1994) Location of M13 coat protein in sodium dodecyl sulfate micelles as determined by NMR. Biochemistry **33**, 12900–12977
46 Jarvet, J., Zdunek, J., Damberg, P. and Gräslund, A. (1997) Three-dimensional structure and position of porcine motilin in sodium dodecyl sulfate micelles determined by ^{1}H NMR. Biochemistry **36**, 8153–8163
47 Bader, R., Bettio, A., Beck-Sickinger, A. G. and Zerbe, O. (2001) Structure and dynamics of micelle-bound neuropeptide Y: comparison with unligated NPY and implications for receptor selection. J. Mol. Biol. **305**, 307–329
48 Wagner, G. and Wüthrich, K. (1982) Amide protein exchange and surface conformation of the basic pancreatic trypsin inhibitor in solution. Studies with two-dimensional nuclear magnetic resonance. J. Mol. Biol. **160**, 343–361
49 Shao, H., Jao, S., Ma, K. and Zagorski, M. G. (1999) Solution structures of micelle-bound amyloid β-(1–40) and β-(1–42) peptides of Alzheimer's disease. J. Mol. Biol. **285**, 755–773
50 Esposito, R., Carver, J. A., Boyd, J. and Campbell, I. D. (1987) High-resolution ^{1}H NMR study of the solution structure of alamethicin. Biochemistry **26**, 1043–1050
51 Glombik, M. M., Krömer, A., Salm, T., Huttner, W. B. and Gerdes, H.-H. (1999) The disulfide-bonded loop of chromogranin B mediates membrane binding and directs sorting from the trans-Golgi network to secretory granules. EMBO J. **18**, 1059–1070

Received 7 March 2002/25 July 2002; accepted 6 August 2002
Published as BJ Immediate Publication 6 August 2002, DOI 10.1042/BJ20020385